# Site-Specific Nitration Differentially Influences $\tau$ Assembly in Vitro[†]

Matthew R. Reynolds,*[,‡] Robert W. Berry,[‡,§] and Lester I. Binder[‡,§]

*Department of Cell and Molecular Biology and Cognitive Neurology and Alzheimer's Disease Center, Feinberg School of Medicine, Northwestern University, Chicago, Illinois 60611*

*Received May 31, 2005; Revised Manuscript Received July 27, 2005*

ABSTRACT: Previously, we reported that the microtubule-associated $\tau$ protein, the major constituent of neurofibrillary tangles (NFTs) in Alzheimer's brain, undergoes site-selective nitration by peroxynitrite ($ONOO^-$) and that this event inhibits $\tau$ polymerization in vitro [Reynolds et al. (2005) *Biochemistry 44*, 1690−1700]. In the present study, we extend our analysis of $\tau$ nitration to include mutant $\tau$ proteins singly nitrated at each residue targeted by $ONOO^-$ in vitro (Tyr18, Tyr29, Tyr197, and Tyr394). Using our polymerization paradigm, we demonstrate that site-specific Tyr nitration differentially alters the rate and/or extent of $\tau$ assembly and generates robust changes in filament morphology. As determined by quantitative electron microscopy, select nitration of residues Tyr29 and Tyr197 increases the average length of synthetic $\tau$ filaments but does not alter the steady-state polymer mass. In contrast, site-specific nitration of residues Tyr18 and Tyr394 decreases the average length and/or number of synthetic filaments, resulting in a significant reduction in filamentous mass and an increase in $\tau$ critical concentration. Intriguingly, affinity measurements demonstrate that nitrative modifications do not preclude formation of the Alz-50 epitope, a pathological $\tau$ conformation detectable in authentic paired helical filaments (PHF$\tau$). In fact, the Alz-50 antibody binds filaments assembled from nitrated mutant $\tau$ with higher avidity than wild-type filaments, even in instances where the overall filamentous mass is reduced. Taken together, our results suggest that site-specific nitration modulates the nucleation and/or elongation capacity of assembly-competent $\tau$ and that assumption of the Alz-50 conformation may be necessary, but not sufficient, to induce filament formation.

Alzheimer's disease (AD)[1] is a progressive amnestic dementia characterized by the pathological self-association of the microtubule-associated $\tau$ protein into filamentous inclusions. The signature fibrillar pathologies of AD include neurofibrillary tangles (NFT), neuritic plaques, and neuropil threads. The NFT, whose distribution in vulnerable brain regions closely correlates with cognitive deficits in patients with AD (*1*, *2*), is largely comprised of the $\tau$ protein assembled into paired helical filaments (PHF) and straight filaments (SF) (*3*−*5*). While PHF$\tau$ is arranged into longitudinal helices with a constant periodicity, SFs lack any demonstrable helical morphology. Insoluble $\tau$ inclusions have also been identified in other non-AD neurodegenerative disorders, including progressive supranuclear palsy (*6*), corticobasal degeneration (*7*), Pick disease (*8*), dementia pugilistica (*9*), Down syndrome (*10*), and frontotemporal dementia and Parkinsonism linked to chromosome 17 (*11*). The observation that $\tau$ deposition is a common denominator among these diverse diseases suggests that $\tau$ dysfunction may represent an end-stage response to a wide variety of neurological insults. The molecular mechanisms governing this process, however, remain largely undefined.

Post-translational phosphorylation (*12*−*14*), glycation (*15*), truncation (*16*), and conformational changes (*17*−*19*) have all been shown to play a role in the series of events leading to fibrillar $\tau$ pathology. In addition, AD-associated inflammation promotes the formation of peroxynitrite ($ONOO^-$), a potent in vivo oxidant capable of Tyr nitration (*20*) and oxidative protein cross-linking via 3,3′-dityrosine (3,3′-DT) linkages (*21*, *22*). Substantial evidence indicates that nitration occurs with biological specificity and can profoundly alter protein folding and function (*23*−*27*). Presumably, the 3-nitrotyrosine (3-NT) moiety modifies protein function by altering the hydrophobicity, hydrogen bonding, and electrostatic properties within the targeted protein. In fact, the function of several proteins implicated in neurodegenerative disease is modulated by nitration of only a single Tyr residue. For example, nitration of Tyr34 by $ONOO^-$ is responsible for inactivation of the human mitochondrial manganese−superoxide dismutase (Mn-SOD) enzyme (*28*). Once this enzyme is inactivated, $O_2^{\bullet-}$ and $NO^{\bullet}$ accumulate in the mitochondrial matrix to form $ONOO^-$ which, in turn, causes cellular damage. Mutations in the SOD gene cause familial amyotrophic lateral sclerosis (ALS), a neurological disease

[†] This work was supported by NIH Awards AG 14453 (L.I.B.), AG 21184 (L.I.B.), and F30 NS051043 (M.R.R.).

* Corresponding author. Phone: (312) 503-0824. Fax: (312) 503-7912. E-mail: m-reynolds@md.northwestern.edu.

[‡] Department of Cell and Molecular Biology.

[§] Cognitive Neurology and Alzheimer's Disease Center.

[1] Abbreviations: AA, arachidonic acid; AD, Alzheimer's disease; ALS, amyotrophic lateral sclerosis; 3,3′-DT, 3,3′-dityrosine; DTPA, diethylenetriaminepentaacetic acid; DTT, dithiothreitol; ELISA, enzyme-linked immunosorbent assay; EM, electron microscopy; HEPES, *N*-(2-hydroxyethyl)piperazine-*N*′-2-ethanesulfonic acid; $i_S$, intensity of scattered light; LLS, right-angle laser light scattering; Mn-SOD, mitochondrial manganese−superoxide dismutase; 3-NT, 3-nitrotyrosine; NFT, neurofibrillary tangle; $ONOO^-$, peroxynitrite; PD, Parkinson's disease; PHF, paired helical filament; SDS−PAGE, sodium dodecyl sulfate−polyacrylamide gel electrophoresis; SEM, standard error of the mean; SF, straight filament; TMB, 3,3′,5,5′-tetramethylbenzidine.

10.1021/bi051028w CCC: $30.25 
Published on Web 10/01/2005

Table 1: Nomenclature and Description of All hτ40 Mutants Used in This Study[a]

| Nomenclature | Description | Purpose |
|---|---|---|
| $^{18}$(n)Y | Nitrated (n) or non-modified hτ40 harboring a single Tyr at Tyr18; i.e., $^{Y}29^{F}$, $^{Y}197^{F}$, $^{Y}310^{F}$, $^{Y}394^{F}$ | To determine whether the non-modified mutant (and the mutant selectively nitrated at residue Tyr18) influences hτ40 assembly |
| $^{29}$(n)Y | Nitrated (n) or non-modified hτ40 harboring a single Tyr at Tyr29; i.e., $^{Y}18^{F}$, $^{Y}197^{F}$, $^{Y}310^{F}$, $^{Y}394^{F}$ | To determine whether the non-modified mutant (and the mutant selectively nitrated at residue Tyr29) influences hτ40 assembly |
| $^{197}$(n)Y | Nitrated (n) or non-modified hτ40 harboring a single Tyr at Tyr197; i.e., $^{Y}18^{F}$, $^{Y}29^{F}$, $^{Y}310^{F}$, $^{Y}394^{F}$ | To determine whether the non-modified mutant (and the mutant selectively nitrated at residue Tyr197) influences hτ40 assembly |
| $^{394}$(n)Y | Nitrated (n) or non-modified hτ40 harboring a single Tyr at Tyr394; i.e., $^{Y}18^{F}$, $^{Y}29^{F}$, $^{Y}197^{F}$, $^{Y}310^{F}$ | To determine whether the non-modified mutant (and the mutant selectively nitrated at residue Tyr394) influences hτ40 assembly |
| $^{310}$Y | Non-modified hτ40 harboring a single Tyr at Tyr310: i.e., $^{Y}18^{F}$, $^{Y}29^{F}$, $^{Y}197^{F}$, $^{Y}394^{F}$ | To determine whether the non-modified mutant influences hτ40 assembly |
| $^{5x}$Y → F | Mutant hτ40 deficient in Tyr residues; i.e., $^{Y}18^{F}$, $^{Y}29^{F}$, $^{Y}197^{F}$, $^{Y}310^{F}$, $^{Y}394^{F}$ | To serve as a negative control for Tyr residues in hτ40 polymerization experiments |

[a] Full-length human τ (hτ40) contains five Tyr residues located at positions Tyr18, Tyr29, Tyr197, Tyr310, and Tyr394.

targeting motor neurons. Moreover, tyrosine hydroxylase, the rate-limiting enzyme in dopamine synthesis, is a nitrative target in models of Parkinson's disease (PD). Nitration of Tyr423 in tyrosine hydroxylase results in enzyme dysfunction with a reduction of dopamine levels in mouse striatum (*29*, *30*).

Several reports have revealed that α-synuclein, a presynaptic protein whose aberrant misfolding results in the accumulation of Lewy bodies in PD brain, is a substrate for $ONOO^-$ (*22*) and that nitration prevents α-synuclein fibrillation (*31*, *32*). Intriguingly, α-synuclein exhibits striking structural and functional similarities to τ, including its natively unfolded structure in solution and its ability to promote microtubule assembly (*33*). Using an antibody raised against nitrated α-synuclein, Giasson et al. have demonstrated robust labeling of the intracellular lesions in PD brain (*34*). Similarly, antibodies reactive toward nitrated τ label both pre-tangles and mature NFTs in post-mortem AD brain (*35*). This latter finding speaks to the potentially dynamic role of τ nitration in tangle evolution and suggests that nitration may be an early event in AD.

Previously, we showed that τ nitration sites fill in a hierarchical fashion following $ONOO^-$ treatment whereby the amino-terminal residues Tyr18 and Tyr29 are preferentially modified prior to residues Tyr197 and Tyr394 (*21*). Furthermore, using our in vitro assembly paradigm, we observed that nitration markedly reduces the ability of wild-type τ to polymerize in vitro (*21*). These previous studies, however, did not delineate the nitrated residues responsible for this inhibitory effect on τ polymerization. In this report, we demonstrate that nitrative modification at *individual* Tyr residues dramatically alters the rate and/or extent of τ polymerization in vitro. Select nitration at Tyr29 and Tyr197 increases the average filament length without changing the steady-state polymer mass. In contrast, nitration at residues Tyr18 and Tyr394 decreases the average filament length and/or number relative to wild-type τ. This translates into an overall reduction in filamentous mass and an increase in τ critical concentration. Surprisingly, site-specific τ nitration does not prevent formation of the Alz-50 epitope, even in instances where nitration decreases the overall polymer mass. Collectively, these data suggest that site-specific nitration may regulate the nucleation and/or elongation of τ filament formation. These findings also provide the first direct evidence that the pathological Alz-50 conformation may be divorced from synthetic filament formation.

## EXPERIMENTAL PROCEDURES

*Mutagenesis, Expression, and Purification of hτ40*. Wild-type and mutant τ proteins were expressed using the pT7C-hτ40 plasmid that drives the expression of full-length human τ (hτ40) fused to an amino-terminal six-His affinity tag (*36*). This plasmid harbors the longest central nervous system isoform of τ (441 residues) containing two amino-terminal insertions as well as differentially spliced exons 2, 3, and 10 (*37*−*39*). The hτ40 cDNA was mutagenized using a site-directed mutagenesis kit (Stratagene) with 33−38-mer primers (Integrated DNA Technologies, Inc.) that define the sequence flanking each targeted codon. Multiple rounds of Tyr → Phe mutagenesis were performed, resulting in quadruple hτ40 mutants that contain single Tyr residues at each position in the native protein (Tyr18, Tyr29, Tyr197, Tyr310, and Tyr394, respectively). A quintuple hτ40 mutant was also engineered to serve as a negative control in all polymerization experiments. Several of these mutants have been described previously (*21*). A detailed summary of all mutants used in this study, along with their adopted nomenclature, is presented in Table 1. The identity and position of all mutations were confirmed by automated DNA sequencing (Center For AIDS Research DNA Sequencing Core, Northwestern University). Wild-type and mutant hτ40 proteins were expressed in *Escherichia coli* strain BL21 (DE3) [$F^-$ *om*pT *hsd*$S_B$ ($r_B^-m_B^-$) *gal dcm*] cells and purified over an immobilized Ni-NTA metal affinity column (Qiagen) (*40*, *41*). Size-exclusion chromatography was subsequently performed to separate full-length hτ40 from incompletely translated hτ40 proteins that retain the six-His affinity tag (*41*).

*Nitration of Mutant hτ40 Proteins*. $ONOO^-$ was prepared from sodium nitrite and acidified $H_2O_2$ as described previously (*42*). Unreacted $H_2O_2$ was removed by passing the $ONOO^-$ stock solution over a manganese dioxide column (*43*). The $ONOO^-$ concentration was measured spectrophotometrically at 302 nm in 0.3 M NaOH ($\epsilon_{302} = 1670\ M^{-1}\ cm^{-1}$) prior to each experiment (*24*). Wild-type and mutant hτ40 proteins were dialyzed against nitration buffer [100 mM potassium phosphate, 25 mM sodium bicarbonate (pH 7.4), and 0.1 mM DTPA] for 16 h at 4 °C. Post-dialysis protein concentrations were determined by the Lowry method using bovine serum albumin as a standard (*44*). A 100-fold molar excess of $ONOO^-$ was added to each mutant protein in two boluses with vigorous stirring for 30 s at room temperature. The final pH was measured and kept at pH 7.4 (*45*).

Following $ONOO^-$ treatment, proteins were concentrated via Centriprep YM-10 filter devices (Millipore) and purified over a Sephacryl S-300 gel filtration column (Amersham Biosciences) to separate nitrated hτ40 monomers from 3,3′-DT cross-linked hτ40 oligomers (*21*). Protein purity was assessed by sodium dodecyl sulfate−polyacrylamide gel electrophoresis (SDS−PAGE) with Coomassie Brilliant Blue staining. Final concentrations of nitrated, monomeric hτ40 were again determined by the Lowry method using bovine serum albumin as a standard (*44*).

*Determination of 3-NT Immunoreactivity in Nitrated hτ40 Mutants*. Enzyme-linked immunosorbent assays (ELISAs) were performed to measure the relative affinity of a 3-NT-specific antibody for either wild-type or nitrated mutant hτ40. Briefly, 100 ng of wild-type or nitrated mutant hτ40 was diluted in borate−saline buffer [100 mM boric acid, 25 mM sodium borate decahydrate, 75 mM NaCl, and 0.05% (w/v) thimerosal] and immobilized onto a 96-well microtitration plate (Corning Inc.). Immobilized proteins were blocked for 1 h in a 5% (w/v) solution of nonfat dry milk in wash buffer [100 mM boric acid, 25 mM sodium borate decahydrate, 75 mM NaCl, 0.05% (w/v) thimerosal, 0.4% (w/v) bovine serum albumin, and 0.05% (w/v) Tween-20] and then incubated for 2 h at room temperature in a polyclonal 3-NT antibody solution (1 μg/mL; Chemicon). Following a secondary incubation with a horseradish peroxidase-conjugated anti-rabbit antibody (Jackson ImmunoResearch), the proteins were reacted with a 3,3′,5,5′-tetramethylbenzidine (TMB) substrate solution for 10 min at room temperature. The reaction was stopped using a 3% (v/v) $H_2SO_4$ solution, and the absorbance of the immunoconjugate was read at 450 nm on a microplate reader (Bio-Tek Instruments, Inc.). We have previously shown that the polyclonal 3-NT antibody cross-reacts to a modest degree with non-modified hτ40 monomer (*21*). For this reason, the absorbance due to cross-reactivity of the 3-NT antibody with non-modified hτ40 was subtracted from all measurements.

*Polymerization Reactions*. Polymerization of hτ40 was induced using the fatty acid arachidonic acid (AA) as previously described (*46*). A working solution of AA was prepared by diluting a 100 mg/mL stock (Cayman Chemicals) in 100% ethanol to a final concentration of 2 mM. All working AA solutions were discarded immediately after use, and stock solutions were kept at −20 °C for no longer than 1 month to prevent oxidation. Wild-type, mutant, and nitrated mutant hτ40 proteins were diluted into polymerization buffer [10 mM *N*-(2-hydroxyethyl)piperazine-*N*′-2-ethanesulfonic acid (HEPES) (pH 7.4), 100 mM NaCl, and 5 mM dithiothreitol (DTT)] to a final concentration of 4 μM. For all $ONOO^-$-treated proteins, nitrated hτ40 monomers were isolated from 3,3′-DT cross-linked oligomers prior to assembly as described above. Polymerization was initiated by adding the AA inducer to a final concentration of 75 μM. Reaction solutions were incubated for 6 h at room temperature without stirring.

*Right-Angle Laser Light Scattering*. Following addition of the AA inducer, polymerization samples (250 μL) were transferred into fluorometer cells (5 mm path length; PGC Scientific) and illuminated with vertically polarized laser light ($\lambda = 488$ nm) generated by a Lexel model 65 ion laser at a setting of 5 mW. Images were captured at a 90° angle to the incident light beam and perpendicular to the direction of polarization using a digital camera (Electrim Corp., model EDC1000HR) operated by HiCam '95 software (written by G. Albrecht-Buehler, Northwestern University; available at http://www.basic.northwestern.edu/g-buehler/hicam.htm). Digital images were collected using an exposure time of 25−50 ms and an aperture setting of F8 to prevent saturation of signal intensity. Laser light scattering (LLS) was monitored over a 6 h period, and background-corrected scattering values were obtained by determining the scattering intensity ($i_S$) at time zero (dark current) and subtracting this value from all measurements. It was previously demonstrated that the amino-terminal affinity tag has no effect on hτ40 polymerization in vitro (*47*). All data were fit by either linear regression, nonlinear regression to one-phase exponential association curves, or Boltzman sigmoidal curves using GraphPad Prism 3.0 software.

*Transmission Electron Microscopy*. Polymerization aliquots were fixed in 2% (w/v) glutaraldehyde for transmission electron microscopy (EM) analysis. Samples were absorbed onto 300 mesh, carbon-coated Formvar grids (Electron Microscopy Sciences), negatively stained using 2% (w/v) uranyl acetate, and analyzed using the JEOL JEM-1220 EM instrument at 60 kV and a magnification of 20000× (*48*). Images were captured using a digital camera (Kodak MegaPlus model 1.6I AMT) controlled by the AMT Camera Controller software package. For each sample, grids were prepared in duplicate, and filament dimensions were quantified from at least six random images per grid (*47*). Images were processed in Adobe Photoshop 7.0, and quantification was performed using Optimas 6.5 software (Media Cybernetics) (*47*). The average mass of filaments per field was determined by multiplying the field's average filament length by the average filament number. The level of statistical significance was set at 0.05, and means were compared using the Student's two-tailed *t* test.

*Determination of Length Distributions*. Length distributions were determined as described previously (*48*, *49*). Briefly, digital electron micrographs were imported into Adobe Photoshop 7.0 where the brightness and contrast were adjusted to optimize visualization (*50*). Images were thresholded using Optimas 6.5 software, and the lengths of individual filaments were automatically traced using the "trace line" feature of the program. These data were extracted into GraphPad Prism 3.0 software, and the frequency distribution of filament lengths formed from wild-type, mutant, and nitrated mutant hτ40 proteins was determined in bins of 100 nm. The center of the first bin was set to 50 nm.

*Critical Concentration Measurements*. Wild-type and nitrated mutant hτ40 proteins were diluted in polymerization buffer [10 mM HEPES (pH 7.4), 100 mM NaCl, and 5 mM DTT] to final concentrations ranging from 2 to 6 μM. We have previously shown that LLS measurements are less reliable when using τ concentrations ≤1 μM (*46*). For this reason, τ concentrations <2 μM were not utilized in our experiments. Polymerization was induced by the addition of AA (75 μM), and all solutions were incubated for 6 h at room temperature without stirring. Maximum scattering intensities were then measured and plotted against protein concentration. Data were fit by linear regression analyses, and the critical concentration of wild-type and nitrated mutant hτ40 proteins was estimated from the abscissa intercept (*46*).

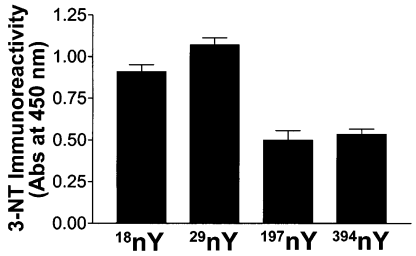


FIGURE 1: 3-NT immunoreactivity of nitrated hτ40 mutants. ELISAs were performed to measure the relative affinity of a 3-NT-specific antibody toward 100 ng of wild-type or nitrated mutant hτ40 protein (see Table 1 for mutant descriptions). The absorbance due to cross-reactivity of the 3-NT antibody with non-modified hτ40 was subtracted from all measurements. Results are from eight independent experiments and are plotted as the mean ± SEM.

*Quantitative Determination of Equilibrium Dissociation Constants*. In-solution affinity constants were calculated using an indirect ELISA method as described previously (*51*). Briefly, varying concentrations of analyte (wild-type or nitrated mutant hτ40), in either monomeric or filamentous form, were incubated in solution with a constant antibody concentration until equilibrium was achieved. To ensure that the total analyte concentration was in large excess over the total antibody concentration, analyte concentrations ranged from ten-fold above the concentration of antibody binding sites to a maximum of 100 nM (*51*). The antibody concentrations used (0.04 nM Alz-50 and 0.025 nM Tau-5) were determined from ELISA calibration curves, which showed a linear dependence in the ranges examined. Following a 16 h incubation at 4 °C in blocking buffer [Tris-buffered saline and 0.2% (w/v) bovine serum albumin], 150 μL of sample was transferred into each well of a microtitration plate preabsorbed with 250 ng/well of wild-type hτ40. An ELISA was then performed to determine the proportion of antibody that remained unsaturated at equilibrium in the original antibody−antigen solution (*51*). The molecular masses of the IgM (pentamer plus linker) and IgG antibodies were estimated at 900 and 150 kDa, respectively.

Scatchard analyses were performed by plotting $\upsilon/a$ as a function of $\upsilon$, where $\upsilon$ is the fraction of bound antibody and $a$ is the concentration of free analyte at equilibrium (*51*). Data were fit by linear regression analyses, and the equilibrium dissociation constants ($K_d$) were calculated from the negative reciprocal of the slope. The fractional occupancy of antibody binding sites was estimated from the abscissa intercept upon extrapolation to zero ordinate (*52*).

## RESULTS

*hτ40 Mutants Containing Single Tyr Residues Are Differentially Nitrated by ONOO⁻*. Previously, we qualitatively determined that, following $ONOO^-$ treatment, τ nitration sites fill in a hierarchical fashion with site selectivity toward residues Tyr18 and Tyr29 (*21*). Therefore, as a first step toward characterizing the effects of site-specific nitration on full-length human τ (hτ40) polymerization, we quantified the relative 3-NT levels of each quadruple Y → F mutant after treatment with a 100-fold molar excess of $ONOO^-$ (Figure 1). A summary of all the hτ40 mutants utilized in this study, along with their adopted nomenclature, is presented in Table 1. It should be noted that a $^{310}$nY mutant was not included in these analyses because we previously showed that $ONOO^-$-mediated nitration infrequently occurs at this position in vitro (*21*). As demonstrated by ELISA, the nitrated hτ40 mutant containing a single Tyr at position Tyr18 ($^{18}$nY) exhibits significantly greater reactivity toward the 3-NT antibody than either the $^{197}$nY or $^{394}$nY proteins [0.91 $A_{450}$ units (± 0.04) versus 0.50 $A_{450}$ units (± 0.06) or 0.53 $A_{450}$ units (± 0.03), respectively; $p < 0.0005$ in both comparisons] (Figure 1). Similarly, the $^{29}$nY mutant shows a two-fold greater 3-NT affinity [1.07 $A_{450}$ units (± 0.04)] than either the $^{197}$nY or $^{394}$nY proteins ($p < 0.00005$ in both comparisons). It should be included that the $^{29}$nY protein exhibits a small, but statistically significant, increase in 3-NT immunoreactivity when compared to the $^{18}$nY mutant ($p < 0.05$). Therefore, although the relative level of nitration on each Tyr residue differs somewhat from our previous results (*21*), the *order of reactivity* remains the same: $ONOO^-$ preferentially nitrates Tyr residues at the amino terminus ($^{18}$nY and $^{29}$nY) as compared with Tyr residues in the proline-rich region of τ ($^{197}$nY) or adjacent to the carboxy terminus ($^{394}$nY).

*Tyr Residues Are Not Required for AA-Induced hτ40 Polymerization*. In an earlier work, we demonstrated that our AA-induced in vitro assembly paradigm accurately models τ polymerization under near-physiological levels of τ concentration, ionic strength, pH, and ambient temperature (*53*). Filaments generated from this paradigm morphologically and immunologically resemble authentic τ filaments derived from post-mortem AD brain (*54*). To examine whether Y → F mutagenesis of hτ40 alters polymerization kinetics relative to the wild-type protein, right-angle laser light scattering (LLS) was used to measure the rate of hτ40 assembly following AA induction. The intensity of scattered light ($i_S$), which is proportional to the mass of filamentous hτ40 in solution (*46*), was plotted as a function of reaction time. The data collected for each non-modified hτ40 mutant displayed an excellent fit to a one-phase exponential association curve ($r^2 = 0.91-0.95$). Equilibrium scattering values for all non-modified mutants were achieved within 6 h, and these values did not differ significantly from the hτ40 control ($i_{S\ h\tau40} = 201.8 \pm 2.3$) (Figure 2A). While the apparent rate of polymerization was similar for all hτ40 mutants, small, but statistically significant, differences in half-maximal scattering values ($t_{1/2}$) were observed between proteins that contained residue Tyr310 (wild-type hτ40 and $^{310}$Y) and those mutants lacking Tyr at this position ($^{18}$Y, $^{29}$Y, $^{197}$Y, $^{394}$Y, and $^{5x}$Y → F). For example, the $t_{1/2}$ value for wild-type hτ40 (4.5 min) was statistically smaller than the $t_{1/2}$ value for $^{18}$nY (9.9 min; Figure 2A). This observation supports previous findings that Y310 lies within a critical interaction motif ($^{306}$VQIVYK$^{311}$) known to be essential for in vitro τ polymerization (*55*).

To examine filament morphology and validate the results obtained by LLS, filaments assembled from non-modified mutant proteins were visualized using transmission EM. Qualitatively, all non-modified hτ40 mutants displayed straight filament (SF) morphology similar to the non-mutated wild-type filaments (data not shown). Quantitatively, the average length, number, and mass of all mutant hτ40 filaments did not significantly differ from the hτ40 control (data not shown). Importantly, filaments assembled from mutant hτ40 proteins lacking all Tyr residues (termed $^{5x}$Y → F, Table 1) were similar to wild-type filaments in both morphology and average filament dimensions. Taken to-

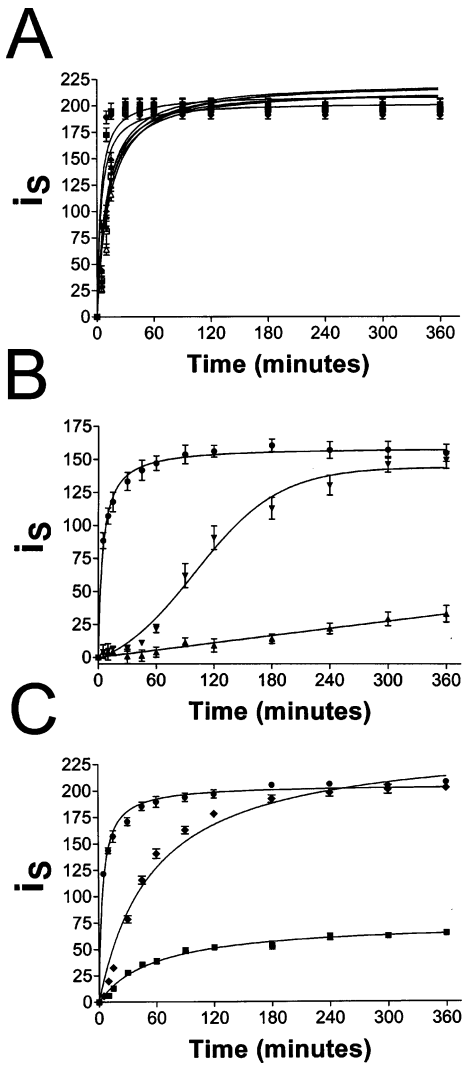


FIGURE 2: Select nitration at individual Tyr residues alters the rate and/or extent of hτ40 polymerization. Wild-type hτ40 was mutagenized to convert four of the five, or five of the five, Tyr residues to Phe (see Table 1 for mutant descriptions). After treatment with a 100-fold molar excess of $ONOO^-$, the nitrated, monomeric proteins were analyzed by laser light scattering to measure the rate of hτ40 assembly following AA induction. (A) The intensity of scattered light ($i_S$) is shown as a function of induction time for wild-type (■) and non-modified mutant [$^{18}$Y (▲), $^{29}$Y (▼), $^{197}$Y (◆), $^{310}$Y (●), $^{394}$Y (□), and $^{5x}$Y → F (△)] hτ40 proteins. (B) Polymerization time course of wild-type (●), $^{18}$nY (▲), and $^{29}$nY (▼) hτ40 proteins. (C) Polymerization time course of wild-type (●), $^{197}$nY (◆), and $^{394}$nY (■) hτ40 proteins. All data were fit by either linear regression, non-linear regression to one-phase exponential association curves, or Boltzman sigmoidal curves. Results are from five independent experiments and are plotted as the mean ± SEM.

gether, these data suggest that genetic ablation of all five Tyr residues in hτ40 produces (1) AA-induced filaments that are morphologically and quantitatively analogous to wild-type filaments and (2) AA-induced assembly kinetics and maximal scattering intensities similar to wild-type hτ40. For these reasons, the Y → F mutants were deemed appropriate reagents to assay for the effects of site-specific nitration on hτ40 polymerization.

*Site-Specific Nitration Alters the Rate and/or Extent of hτ40 Polymerization.* LLS experiments were then performed using hτ40 mutants singly nitrated at residues Tyr18, Tyr29, Tyr197, and Tyr394. As evidenced from the polymerization time course, site-specific nitration at Tyr18 ($^{18}$nY) greatly

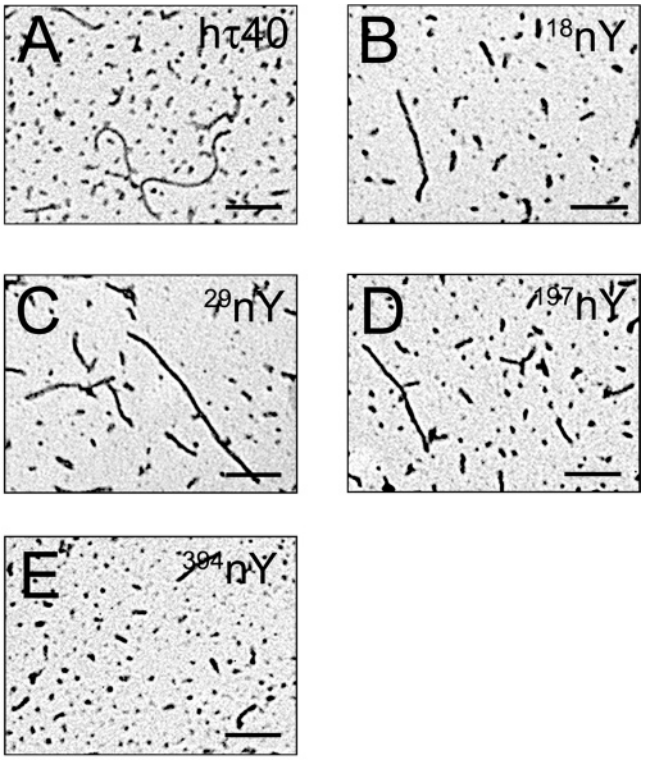


FIGURE 3: Site-specific nitration of hτ40 alters synthetic filament morphology. Negative-stain electron micrographs were acquired from wild-type (A) and nitrated mutant hτ40 filaments [$^{18}$nY (B), $^{29}$nY (C), $^{197}$nY (D), and $^{394}$nY (E)] following a 6 h induction period. Micrographs are representative of five independent experiments. The size bar represents 250 nm.

diminishes light scattering levels relative to wild-type hτ40 and demonstrates linear assembly kinetics (Figure 2B). This finding likely translates into a significantly reduced polymer mass for the $^{18}$nY protein. Half-maximal scattering values ($t_{1/2}$) for the $^{18}$nY mutant could not be obtained because steady state was not achieved within the duration of these experiments. In contrast, while the $^{29}$nY protein approaches the maximal scattering intensity of wild-type hτ40, its kinetic profile differs markedly from the hτ40 control. An excellent fit to a sigmoidal curve is obtained from the $^{29}$nY mutant scattering data ($r^2 = 0.96$) that displays a considerable lag time prior to reaching the plateau. This lag time results in a lengthening of the $t_{1/2}$ value from 5.4 min for wild-type hτ40 to 100.2 min for $^{29}$nY (Figure 2B). King et al. have previously demonstrated that AA-induced hτ40 polymerization proceeds through a condensation reaction whereby filament nucleation is followed by elongation of the nascent polymer (*54*). Within this model system, the apparent lag time approximates the rate of filament nucleation (*56*). Accordingly, the marked increase in lag time observed during the $^{29}$nY polymerization time course may indicate a deficit in polymer nucleation.

Select nitration at Tyr197 ($^{197}$nY) delays the $t_{1/2}$ value from 4.8 min for wild-type hτ40 to 40.4 min (Figure 2C). The maximum scattering intensity for $^{197}$nY, however, does not differ significantly from the hτ40 control, and the data fit well to a one-phase exponential association curve ($r^2 = 0.97$). hτ40 proteins singly nitrated at position Tyr394 ($^{394}$nY) scatter laser light far less efficiently than the wild-type control and demonstrate a large increase in $t_{1/2}$ at 41.6 min (Figure 2C). Unlike the polymerization time course for the $^{18}$nY

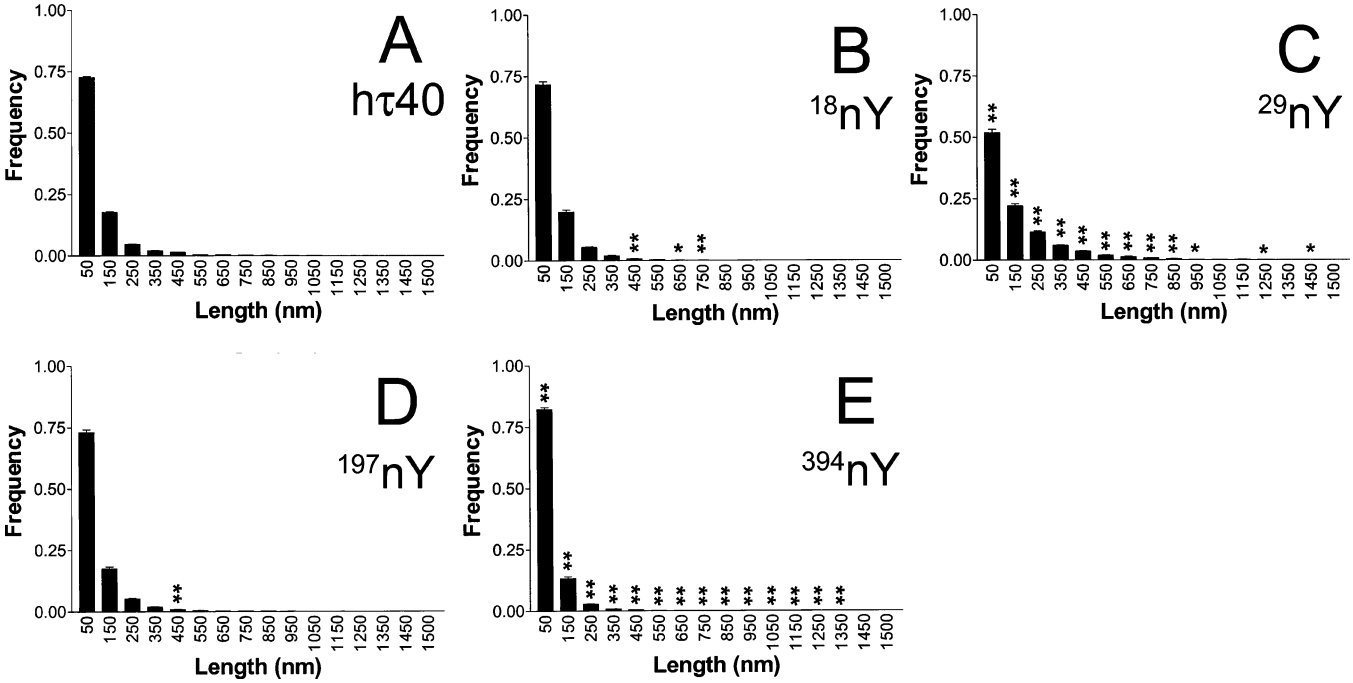


FIGURE 4: Site-specific hτ40 nitration differentially influences synthetic filament length. Frequency distributions of polymer length were measured for wild-type (A) and nitrated mutant hτ40 [$^{18}$nY (B), $^{29}$nY (C), $^{197}$nY (D), and $^{394}$nY (E)] following a 6 h induction period. Digital micrograph images (similar to those shown in Figure 3) were thresholded using Optimas 6.5 software, and the lengths of individual filaments were automatically traced using the "trace line" feature of the program. Data were imported into GraphPad Prism 3.0 software, and filaments were sorted into bins of 100 nm. The center of the first bin was set to 50 nm. Results are from five independent experiments and are plotted as the mean ± SEM. The Student's two-tailed *t* test was used to compare the mean lengths of wild-type and nitrated mutant hτ40 filaments in each bin (* $p < 0.05$; ** $p < 0.005$).

mutant, however, the LLS data collected from the $^{394}$nY protein fit a one-phase exponential association curve and display a maximal scattering intensity of 57.5 ± 3.4 at steady state. Intriguingly, while the $^{18}$nY and $^{394}$nY mutant proteins both attenuate maximal $i_S$ values relative to the hτ40 control, nitration of wild-type hτ40 inhibits polymerization to a greater extent than either of these mutants alone (see data from ref *21*). These results suggest that nitration of individual Tyr residues alters the rate and/or extent of AA-induced hτ40 polymerization and that nitration of multiple Tyr residues may have a combinatorial effect on hτ40 assembly. Further, select nitration of the extreme amino- or carboxy-terminal Tyr residues reduces light scattering to the greatest extent in vitro.

*Site-Specific Nitration Alters Filament Morphology*. To confirm that our LLS data are attributable to the formation of bona fide τ filaments, we examined filament ultrastructure by transmission EM. As shown from the electron micrographs, wild-type hτ40 filaments demonstrate two morphologically distinct structures: (1) small, globular aggregates measuring ~25−50 nm in their longest axis and (2) long, rod-like structures with straight filament (SF) morphology ranging in length from ~100 to 1000 nm (Figure 3A). The former aggregate most likely represents nucleation centers that have not yet undergone elongation or are elongation-incompetent (described in ref *54*). Furthermore, while synthetic filaments assembled from wild-type hτ40 appear sigmoidal in appearance (Figure 3A), the majority of nitrated mutant filaments are linear (Figure 3B−E). This apparent linearity may indicate a lack of polymer flexibility relative to wild-type hτ40 filaments.

Qualitatively, the average length of synthetic filaments assembled from the $^{18}$nY protein appears to be similar to that of wild-type hτ40 (Figure 3B). However, the number of $^{18}$nY filaments per field is markedly decreased relative to the non-modified hτ40 filaments. In contrast, filaments derived from the $^{29}$nY mutant exhibit a paucity of small, globular aggregates (Figure 3C). This decrease in putative nucleation centers, which is consistent with the increased lag time observed during the $^{29}$nY polymerization time course (Figure 2B), accompanies a greater number of qualitatively longer filaments (Figure 3C). In fact, the mature $^{29}$nY filaments were greater in length than any other of the filaments examined. Filaments assembled from the $^{197}$nY mutant appear qualitatively similar, in both length and number, to the wild-type hτ40 filaments (Figure 3D). Polymerization of hτ40 proteins singly nitrated at residue Tyr394 ($^{394}$nY), however, yields small globular aggregates with very few elongated filaments. This predominance of putative nucleation centers possibly indicates a reduced capacity for elongation. Taken together, these data suggest that site-specific hτ40 nitration produces robust changes in filament morphology by modulating filament elongation and/or nucleation.

*Site-Specific Nitration at Tyr29 and Tyr394 Alters Nascent Filament Length*. The qualitative estimations of filament length presented above were quantified by measuring filament length distributions in the wild-type and nitrated mutant hτ40 proteins (Figure 4). Filaments were sorted into bins of 100 nm where the center of the first bin was set to 50 nm. As shown from the histograms, the majority of the hτ40 polymer [72.6% (± 0.01%)], and therefore most of the wild-type filament mass, was comprised of aggregates ≤100 nm in length (Figure 4A). These small aggregates appear to be similar to the amorphous, globular structures that represent nucleated, but not elongated, filaments (described in ref *54*).

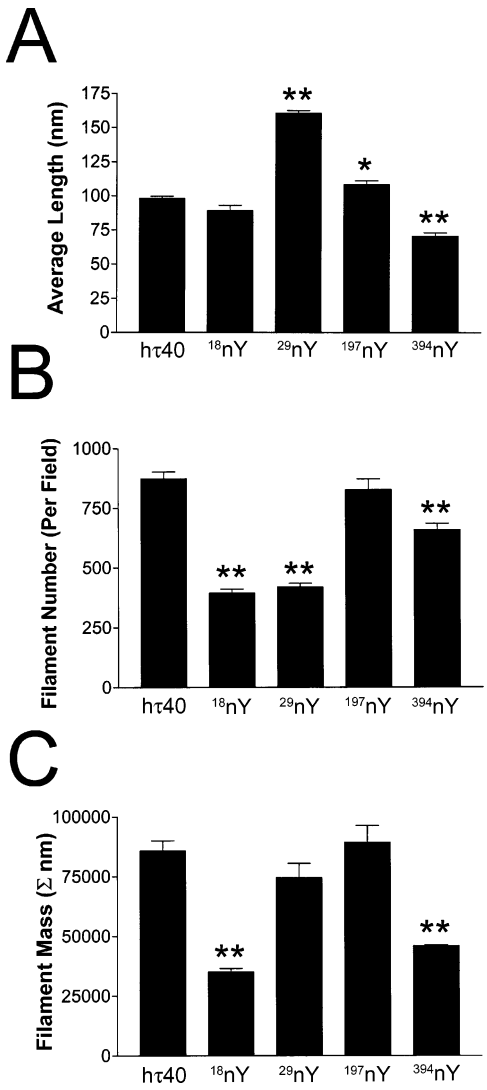


FIGURE 5: Nitration of Tyr18 and Tyr394 decreases AA-induced polymer mass. Quantitative EM measurements from wild-type and nitrated mutant hτ40 filaments were performed following a 6 h induction period. The average length (A), number (B), and mass (C) of filaments per field were determined for wild-type and nitrated mutant hτ40. Results are from five independent experiments and are plotted as the mean ± SEM. The Student's two-tailed *t* test was used to compare the mean dimensions of wild-type and nitrated mutant hτ40 filaments (* $p < 0.05$; ** $p < 0.005$).

Wild-type hτ40 filaments were found to have lengths up to 1350 nm. However, these longer filaments constituted only a small fraction of the overall filament mass. Select nitration at the amino-terminal residue Tyr18 generated small, but statistically significant, decreases in the frequency of longer length filaments (400−700 nm) relative to wild-type filaments (Figure 4B). In contrast, the length distributions of filaments assembled from $^{29}$nY display a marked shift toward longer filaments (Figure 4C). Only 51.9% (± 0.09%) of the $^{29}$nY filaments were ≤100 nm in length, and the majority of polymer mass was distributed over longer length filaments. In fact, filaments assembled from the $^{29}$nY mutant reached up to 1850 nm in length. As predicted from the qualitative EM analyses, filaments comprised of $^{197}$nY monomers exhibit a very similar length distribution profile to wild-type hτ40 filaments (Figure 4D). On the other hand, the frequency distributions of $^{394}$nY filament length show a significant shift toward small, globular aggregates (Figure 4E). The majority

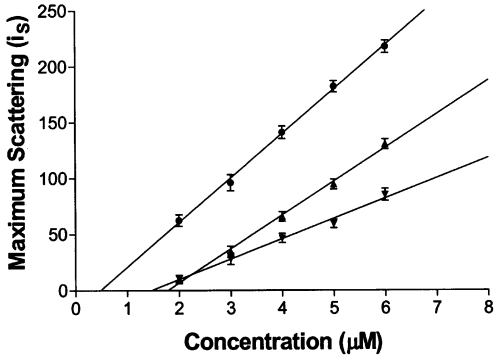


FIGURE 6: Nitration of Tyr18 and Tyr394 increases hτ40 critical concentration. Polymerization experiments were performed using varying concentrations (2−6 μM) of wild-type (●), $^{18}$nY (▲), and $^{394}$nY (▼) hτ40 proteins, and the maximal scattering intensities were measured following 6 h. Data are plotted as maximal light scattering as a function of protein concentration. The critical concentration of each protein was calculated from the abscissa intercept. Results are from five independent experiments and are plotted as the mean ± SEM.

of $^{394}$nY filament mass was sequestered within the ≤100 nm length bin, and no measured filaments were greater than 850 nm in length (Figure 4E). Taken together, these data suggest that nitration of select Tyr residues alters synthetic filament length, perhaps by modulating the nucleation and/or elongation of AA-induced hτ40 filaments.

*Site-Specific Nitration at Tyr18 and Tyr394 Decreases AA-Induced Polymer Mass*. To further characterize the effects of site-selective nitration on hτ40 filament formation, we employed transmission EM to quantify the filament dimensions of each nitrated mutant. To this end, the average length, number, and mass of wild-type and nitrated mutant hτ40 filaments were calculated from a random series of electron micrographs similar to those shown in Figure 3. The data show that while AA-induced $^{18}$nY assembly does not alter filament length relative to hτ40 (Figure 5A), nitration at this position reduces the average filament number (393.9 ± 16.4) to less than half that of wild-type hτ40 (873.2 ± 16.4) (Figure 5B). This reduction in filament number translates into a significant diminution in polymer mass for the $^{18}$nY mutant (Figure 5C). In agreement with the length distribution data, nitration at Tyr29 significantly increases the average filament length per field from 98.0 (± 1.6) nm to 160.5 (± 2.1) nm (Figure 5A). However, because the average filament number for the $^{29}$nY mutant is less than half that of wild-type (419.7 ± 14.7 vs 873.2 ± 28.8, respectively), the steady-state values of polymer mass for $^{29}$nY do not differ significantly from hτ40 (Figure 5B,C). As predicted, both nitrated mutants that increase the average filament length ($^{29}$nY and $^{197}$nY) also demonstrate a pronounced lag time, or increase in $t_{1/2}$ values, during the LLS time courses (Figure 2B,C).

Filaments assembled from the $^{197}$nY mutant exhibit a small, but significant, increase in polymer length as compared to the hτ40 control (Figure 5A). These longer filaments, however, do not increase the overall filament mass for the $^{197}$nY protein (Figure 5C). By comparison, site-specific nitration at the more carboxy-terminal residue Tyr394 decreases both the length (70.5 ± 2.5 nm) and number (657.6 ± 26.6) of filaments, resulting in a marked reduction of the average filament mass (45979.8 ± 398.1 nm). Consistent with our polymerization time course data that show decreased

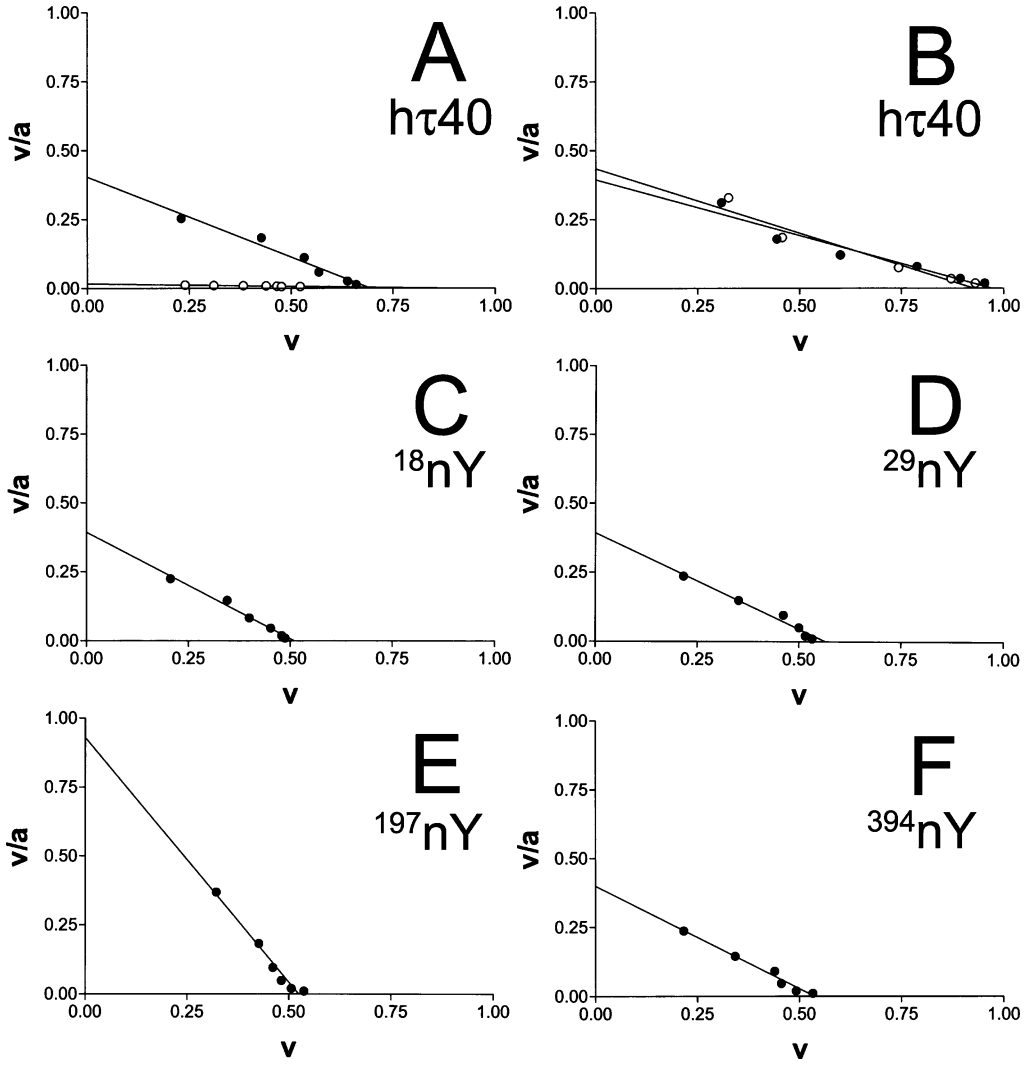


FIGURE 7: Site-specific 3-NT modification does not prevent formation of the Alz-50 epitope. Monoclonal antibodies raised against conformation-specific (Alz-50) or conformation-insensitive (Tau-5) $\tau$ epitopes were incubated in solution with a large excess of wild-type or nitrated mutant h$\tau$40 (in either polymeric or monomeric form) until equilibrium was achieved. An indirect ELISA was then performed to measure the fraction of unbound antibody at equilibrium. Data were fit by linear regression and represented as Scatchard plots, where $\upsilon$ is the fraction of bound antibody and $a$ is the concentration of free analyte at steady state. (A) Scatchard plot of Alz-50 affinity for filamentous (●) and monomeric (○) wild-type h$\tau$40. (B) Scatchard plot of Tau-5 affinity for filamentous (●) and monomeric (○) wild-type h$\tau$40. Scatchard plots of Alz-50 affinity for $^{18}$nY (C), $^{29}$nY (D), $^{197}$nY (E), and $^{394}$nY (F) mutant filaments. A summary of all affinity measurements is presented in Table 2. Results are representative of five independent experiments, and error bars have been omitted for clarity.

maximal scattering for the $^{18}$nY and $^{394}$nY mutants (Figure 2), nitration of the extreme amino- and/or carboxy-terminal Tyr residues greatly attenuates AA-induced filament production.

*Site-Specific Nitration at Tyr18 and Tyr394 Increases h$\tau$40 Critical Concentration*. To determine whether specific nitrative events alter the minimal h$\tau$40 concentration required for self-assembly in vitro (*57*), we estimated critical concentrations using LLS. Using this approach, AA-induced polymerization was performed at varying protein concentrations (2−6 $\mu$M), and the maximal scattering intensity was measured following 6 h (Figure 6). Data were fit by linear regression analyses, and the critical concentration was estimated from the abscissa intercept upon extrapolation to zero ordinate (*46*). Only the $^{18}$nY and $^{394}$nY mutants were used for these analyses because nitration at these sites was shown to decrease the filamentous mass of h$\tau$40 (Figure 5C). As predicted, a linear relationship exists between maximum $i_S$ and wild-type h$\tau$40 concentration, where the abscissa intercept, and therefore critical concentration, was estimated at 0.47 ± 0.14 $\mu$M. This value of h$\tau$40 critical concentration closely agrees with previous reports (*46*, *54*). In contrast, the critical concentrations for the $^{18}$nY (1.78 ± 0.14 $\mu$M) and $^{394}$nY (1.45 ± 0.09 $\mu$M) mutant proteins were three-fold greater than the value calculated for wild-type h$\tau$40 (Figure 6). Consistent with the reduction of polymer mass obtained with the $^{18}$nY and $^{394}$nY mutants (Figure 5C), these data demonstrate that, following nitration of residues Tyr18 and Tyr394, a three-fold greater monomer concentration must be present to support h$\tau$40 polymerization in vitro. This finding suggests that nitration of the extreme amino- and/or carboxy-terminal Tyr residues shifts the polymerization equilibrium toward the monomeric form.

*Site-Specific Nitration Does Not Preclude Formation of the Alz-50 Epitope*. Work from our laboratory has demonstrated that $\tau$ undergoes an ordered sequence of conformational changes during tangle evolution (*17*−*19*). In early-stage tangles, $\tau$ adopts a conformation whereby its amino

Table 2: Summary of Binding Affinity Measurements As Determined from Scatchard Analyses

| Analyte | Antibody | $K_d$ (nM) | Abscissa intercept[a] |
|---|---|---|---|
| Monomeric h$\tau$40 | Tau-5 | $2.50 \pm 0.15$ | $0.90 \pm 0.01$ |
| Filamentous h$\tau$40 | Tau-5 | $2.58 \pm 0.20$ | $0.99 \pm 0.01$ |
| Monomeric h$\tau$40 | Alz-50 | $54.23 \pm 2.69$ | $0.92 \pm 0.02$ |
| Filamentous h$\tau$40 | Alz-50 | $1.75 \pm 0.04$ | $0.70 \pm 0.01$ |
| Filamentous $^{18}$nY | Alz-50 | $1.24 \pm 0.03$ | $0.48 \pm 0.02$ |
| Filamentous $^{29}$nY | Alz-50 | $1.44 \pm 0.02$ | $0.57 \pm 0.01$ |
| Filamentous $^{197}$nY | Alz-50 | $0.61 \pm 0.02$ | $0.53 \pm 0.01$ |
| Filamentous $^{394}$nY | Alz-50 | $1.31 \pm 0.02$ | $0.52 \pm 0.01$ |

[a] Abscissa intercept values approximate the fractional occupancy of antibody binding sites at saturating h$\tau$40 concentrations.

terminus folds back upon the third microtubule-binding repeat. This event coincides with early filamentous changes in $\tau$ and is detected by the conformation-sensitive antibody Alz-50 (*36*, *58*). Therefore, to test the hypothesis that select nitration of the amino-terminal Tyr residues (Tyr18 and Tyr29) sterically hinders the Alz-50 conformation, we measured the binding affinity [or equilibrium dissociation constants ($K_d$)] of the Alz-50 (*59*) and Tau-5 (*60*) antibodies toward wild-type and nitrated mutant h$\tau$40 filaments. Each antibody was incubated in solution with a large excess of analyte until equilibrium was attained. An indirect ELISA was then performed to measure the quantity of antibody that remained unsaturated at equilibrium.

In all cases, Scatchard analyses of these data reveal a linear relationship with $r^2$ values ranging from 0.92 to 0.97. This linearity suggests a lack of cooperative binding between the various forms of h$\tau$40 and the antibodies employed (*52*). As reported previously (*54*), the conformation-dependent Alz-50 antibody exhibits a significantly greater affinity for synthetic h$\tau$40 filaments ($K_d = 1.75 \pm 0.04$ nM) than for monomeric h$\tau$40 ($54.23 \pm 2.69$ nM) (Figure 7A; $K_d$ values are summarized in Table 2). This observation is in agreement with reports showing that the Alz-50 antibody binds a discontinuous, conformationally-sensitive epitope similar to that displayed in authentic PHF$\tau$ (*36*). By comparison, our data reveal that the Tau-5 antibody has similar binding affinities for both monomeric ($2.50 \pm 0.15$ nM) and polymeric ($2.58 \pm 0.20$ nM) h$\tau$40 (Figure 7B; Table 2). Moreover, binding affinity measurements demonstrate a near-complete fractional occupancy of Tau-5 binding sites at saturating concentrations of h$\tau$40 monomer and polymer ($0.90 \pm 0.01$ and $0.99 \pm 0.01$, respectively). These data are consistent with the Tau-5 antibody binding a conformationally-independent, linear epitope that recognizes all h$\tau$40 forms equally (*36*).

Intriguingly, when compared to the $K_d$ value for wild-type filaments, filaments assembled from the $^{18}$nY mutant display a significant increase in binding affinity toward the Alz-50 antibody ($1.24 \pm 0.03$ nM) (Figure 7C, Table 2). The increase in Alz-50 binding affinity demonstrated by the $^{18}$nY filaments is also manifest by the other nitrated mutant filaments (Table 2). However, this increased affinity toward Alz-50 is most pronounced for the $^{197}$nY mutant, which shows nearly a three-fold decrease in $K_d$ value relative to non-modified h$\tau$40 filaments. This finding is particularly surprising given that our data show a *decrease* in the overall amount of polymeric mass for several of the nitrated mutants ($^{18}$nY and $^{394}$nY; Figure 5C). Moreover, the fraction of Alz-50 binding sites occupied by nitrated mutant filaments is less than the value obtained for wild-type h$\tau$40 filaments (Table 2), suggesting that Alz-50 binds the nitrated mutant filaments with greater affinity despite the fact that $\sim$13−22% fewer antibody binding sites are engaged. Taken together, these findings suggest that site-specific h$\tau$40 nitration does not prevent formation of the Alz-50 epitope and that assumption of the Alz-50 conformation may not necessarily lead to filament formation.

## DISCUSSION

Post-translational nitrative modifications have been shown to functionally modify proteins in a biologically specific and site-selective manner (*23*−*27*). $ONOO^-$, thought by many to be the principal in vivo nitrating agent, targets protein Tyr residues, and the resulting reaction product, 3-NT, serves as a biochemical index of $ONOO^-$-mediated damage (*20*). Previous work from our own laboratory has shown that, following $ONOO^-$ treatment, the amino-terminal Tyr residues of $\tau$ (Tyr18 and Tyr29) are nitrated preferentially over residues located in the proline-rich region (Tyr197) and the extreme carboxy terminus (Tyr394) (*21*). Moreover, we have demonstrated that the cumulative effect of $ONOO^-$-mediated $\tau$ nitration is to inhibit in vitro polymerization (*21*). These data, combined with other reports that $\tau$ nitration may be an early event in AD pathogenesis (*35*), suggest that nitrative modifications can prevent the pathological self-association of $\tau$ into filamentous aggregates.

In the present study, we examine the effects of nitration at *individual* Tyr residues on $\tau$ polymerization in vitro. Our data reveal that (1) nitration of single Tyr residues differentially influences the rate and/or extent of $\tau$ assembly and induces robust changes in filament morphology, (2) nitration of residues Tyr29 and Tyr197 increases filament length without altering steady-state polymer mass, (3) nitration of residues Tyr18 and Tyr394 decreases the length and/or number of $\tau$ filaments, resulting in a significant reduction of filamentous mass and an increase in $\tau$ critical concentration, and (4) site-specific Tyr nitration does not preclude formation of the Alz-50 epitope. Collectively, these data suggest that nitration of *specific* Tyr residues alters the nucleation and/or elongation capacity of assembly-competent $\tau$ and generates marked changes in $\tau$ polymerization kinetics.

*Nitration of Individual Tyr Residues Influences $\tau$ Nucleation and/or Elongation.* As first characterized by King et al. (*54*), AA-induced $\tau$ polymerization proceeds through a ligand-mediated mechanism. The initial step in this process involves $\tau$ binding to the anionic surface of AA micelles to assume an assembly-competent conformation (*61*−*63*). Rapid nucleation then occurs, followed shortly thereafter by extension of the nascent polymer into mature filaments. Importantly, both the nucleation and elongation events involve a critical energy barrier that must be overcome before polymerization can occur (*63*).

In this report, we show that nitration of individual Tyr residues modulates the ability of $\tau$ to nucleate and/or elongate filaments. Our data demonstrate that select nitration of the amino-terminal residue Tyr18 negatively regulates nucleation and elongation to an equal extent. This results in filaments that are similar in length, but reduced in number, as compared to wild-type filaments. In contrast, assembly of the $^{29}$nY

mutant results in quantitatively longer filaments with a concomitant reduction in putative nucleation centers. This finding suggests that while the $^{29}$nY mutant is fully competent to elongate filaments, its capacity for nucleation is diminished. This nucleation deficit is further manifest by a prolonged $t_{1/2}$ value in the $^{29}$nY polymerization time course.

The functional domains harboring each Tyr residue may provide insights into the nucleation and/or elongation deficits of the nitrated $\tau$ mutants. For example, residues Tyr18 and Tyr29 lie within the amino terminus of the $\tau$ molecule, a region purported to interact with numerous cellular components, including plasma membranes (*64*−*66*). One possible explanation for how nitration at Tyr18 and/or Tyr29 inhibits nucleation in vitro is that this region facilitates the obligate binding of $\tau$ to AA during assembly. If so, then nitration at these residues would increase the net negative charge at the amino terminus and electrostatically repel this region from the anionic surface of AA micelles. This event would effectively deter $\tau$ from assuming the assembly-competent form requisite for nucleation.

While the AA micelle likely promotes $\tau$ filament formation in vitro (*54*), other fatty acid-like inducers, such as polyanionic lipids, may assume this role in vivo. In fact, EM analyses of post-mortem AD brain demonstrate that many $\tau$ filaments arise from, or end within, the plasma membrane (*67*). It is entirely possible, then, that nitration of the amino-terminal residues Tyr18 and Tyr29 inhibits the binding of $\tau$ to a filament-inducing surface in vivo. The finding that both the $^{18}$nY and $^{29}$nY mutants prevent nucleation to similar degrees (Figure 5B) may be attributable to the proximity of their 3-NT groups to the extreme amino terminus.

In this regard, it is important to note that removal of the extreme amino terminus ($\Delta$2−18) inhibits in vitro $\tau$ assembly (*49*). This finding supports a facilitative role for the amino terminus in $\tau$ polymerization, likely by its contribution to the Alz-50 conformation. Therefore, it is also conceivable that nitration of Tyr18 and/or Tyr29 disrupts this facilitative conformation of $\tau$, precipitating deficits in filament nucleation and/or elongation.

Polymerization of the $^{394}$nY mutant yields putative nucleation foci in the absence of extended filaments. This finding speaks to the potential elongation deficits of the $^{394}$nY mutant. Based upon the Oosawa model of nucleated polymerization (*68*), nucleation would occur by the sequential addition of monomers, each forming a single contact with one another. An association constant, $K_n$, typifies this monomer−monomer interaction. Filament extension, however, not only involves the apposition of adjacent monomers but also requires additional inter-monomer associations. The existence of a critical concentration for h$\tau$40 assembly implies that the association constant for extension, $K_p$, is necessarily greater than $K_n$ due to energetically favorable interactions among subunits. It is entirely possible, therefore, that the $^{394}$nY mutant assumes a conformation that is amenable to nucleation but is inhibitory toward elongation. Consequently, the value of $K_p$ for the $^{394}$nY assembly reaction will be increased ($K_p'$). This would result in a nucleation-competent, elongation-deficient, $\tau$ mutant that can overcome the free energy threshold of $K_n$ to form nuclei but is unable to overcome the kinetic barrier necessary for inter-subunit associations ($K_p'$). Nitration of Tyr394 in vivo, however, may be an infrequent event due to steric hindrance from a phosphate group at Ser396 in the hyperphosphorylated state [PHF-1 epitope (*69*)] or carboxy-terminal truncation events that remove this residue (*19*). Moreover, a recent report demonstrates that Tyr394 serves as a phosphorylation substrate in Alzheimer's brain (*70*).

It is important to include that the degree of 3-NT modification following $ONOO^-$ treatment (Tyr29 > Tyr18 ≫ Tyr394 > Tyr197) does not correlate with the effect of each nitrated mutant on $\tau$ polymerization. For example, while Tyr18 and Tyr29 are modified to the greatest extent in vitro, the $^{18}$nY and $^{29}$nY mutants have entirely disparate effects on $\tau$ polymerization. In fact, Tyr394, which is nitrated to a far lesser extent than either Tyr18 or Tyr29, may have the greatest influence on $\tau$ assembly. Thus, it appears that the *site* of nitration, and not the *degree* of nitration, determines the impact on $\tau$ polymerization in vitro.

*Nitration of Individual Tyr Residues Does Not Preclude Formation of the Alz-50 Epitope*. We have previously shown that the $\tau$ molecule undergoes dynamic conformational rearrangements prior to its pathological self-assembly (*17*−*19*). One of the earliest immunological markers of $\tau$ misfolding, both in vitro and in situ, is the Alz-50 conformation. The discontinuous Alz-50 epitope (residues 5−15, 312−322) is formed when the amino terminus of $\tau$ comes into close apposition with the third microtubule-binding repeat (*36*). This conformational state change is accompanied by the transformation of $\tau$ from a random coil structure into $\beta$-pleated sheets (*71*).

Contrary to our hypothesis that nitration of individual Tyr residues sterically inhibits the Alz-50 epitope, we demonstrate that filaments assembled from nitrated $\tau$ mutants exhibit increased affinity toward the Alz-50 antibody. This observation holds true even when nitration reduces the overall polymer mass ($^{18}$nY and $^{394}$nY). These data provide the first direct evidence that the Alz-50 epitope is not dependent upon the formation of bona fide $\tau$ filaments and can be assumed in the absence of long, rod-like polymers. This finding, however, is in agreement with in situ immunohistochemical data showing that the Alz-50 conformation may indeed be the first pre-filament step toward polymer formation (*19*).

Intriguingly, filaments assembled from the $^{197}$nY mutant have nearly a three-fold greater equilibrium binding affinity toward the Alz-50 antibody than wild-type h$\tau$40 filaments. The Tyr197 residue lies within a proline- and glycine-rich region of the $\tau$ molecule believed to impart the flexibility needed for conformational changes to occur (*72*). In fact, $\tau$ isoforms lacking both of the amino-terminal repeats immediately upstream from the proline-rich region (i.e., h$\tau$23 and h$\tau$24) do not form rod-like filaments (*47*), presumably due to inadequate molecular spacing for the Alz-50 folding event. Accordingly, if nitration at the Tyr197 site "locks" the proline-rich region into a conformation conducive to Alz-50 formation, this event may explain why the $^{197}$nY filaments exhibit an enhanced binding affinity toward the Alz-50 antibody. Our observation that filaments assembled from the $^{197}$nY mutant are morphologically linear, suggesting a reduced flexibility relative to wild-type filaments, supports this contention.

*Neuroinflammation as a Protective Mechanism against $\tau$ Filament Formation*. Neuroinflammation and nitrative injury are prevalent features of AD-affected brain (reviewed in ref *73*). During $\beta$-amyloid-associated inflammation, reactive

microglia upregulate the expression of inducible nitric oxide synthase (iNOS) to generate high levels of nitric oxide ($NO^{\bullet}$) (*74*, *75*). A subset of cortical neurons also contributes to $NO^{\bullet}$ production, albeit to a lesser extent, by constitutive expression of the neuronal NOS isoform (nNOS) (*76*). Reaction of $NO^{\bullet}$ with superoxide anions ($O_2^{\bullet-}$) leads to the formation of $ONOO^-$, a powerful oxidant capable of nitrating protein Tyr residues. While inflammatory sequelae are thought to be beneficial in an acute setting, chronic, unregulated production of reactive nitrogen and oxygen species has been shown to play a mechanistic role in neurodegeneration (*77*−*79*).

Under physiological conditions, intracellular concentrations of τ approximate 2−4 μM (*72*), the majority of which [>99% (*54*)] is tightly bound to the microtubule network. Numerous post-translational events, most notably phosphorylation, can displace τ from the microtubule and increase the pool of free τ available for polymerization (*80*, *81*). Zhang and colleagues recently reported that nitration by $ONOO^-$ also reduces the ability of τ to bind and stabilize microtubules in vitro (*82*). If this free cytoplasmic τ concentration exceeds the threshold for polymerization ($h\tau 40_{crit\ conc} \sim 0.5\ \mu M$; Figure 6), then self-assembly will occur. One potential in vivo correlate to our findings is that, in early-stage AD, nitrotyrosination may compete with aberrant phosphorylation for limiting amounts of τ substrate. In the latter event, hyperphosphorylation would likely increase the concentration of unbound τ and promote an assembly-competent state prone to fibrillation. Alternatively, nitration at specific Tyr residues (Tyr18 and Tyr394) would increase the critical concentration of τ and shift the polymerization equilibrium toward the monomeric state.

Taken together, the data presented herein show that nitrative modification of select Tyr residues abrogates τ assembly in vitro and may provide a neuroprotective mechanism against NFT formation in vivo. These findings have significant implications for AD by revealing a novel pathway through which neuroinflammation may attenuate τ aggregation.

## ACKNOWLEDGMENT

We gratefully acknowledge Robert H. Weir for technical assistance with laser light scattering and Robert Hunter for inspiration and critical reading of the manuscript.

## REFERENCES

1. Arriagada, P. V., Growdon, J. H., Hedley-Whyte, E. T., and Hyman, B. T. (1992) Neurofibrillary tangles but not senile plaques parallel duration and severity of Alzheimer's disease, *Neurology 42*, 631−639.
2. Braak, H., and Braak, E. (1991) Neuropathological stageing of Alzheimer-related changes, *Acta Neuropathol. (Berlin) 82*, 239−259.
3. Kidd, M. (1963) Paired helical filaments in electron microscopy of Alzheimer's disease, *Nature 197*, 192−193.
4. Kosik, K. S., Joachim, C. L., and Selkoe, D. J. (1986) Microtubule-associated protein tau (tau) is a major antigenic component of paired helical filaments in Alzheimer disease, *Proc. Natl. Acad. Sci. U.S.A. 83*, 4044−4048.
5. Wischik, C. M., Novak, M., Edwards, P. C., Klug, A., Tichelaar, W., and Crowther, R. A. (1988) Structural characterization of the core of the paired helical filament of Alzheimer disease, *Proc. Natl. Acad. Sci. U.S.A. 85*, 4884−4888.
6. Tabaton, M., Whitehouse, P. J., Perry, G., Davies, P., Autilio-Gambetti, L., and Gambetti, P. (1988) Alz 50 recognizes abnormal filaments in Alzheimer's disease and progressive supranuclear palsy, *Ann. Neurol. 24*, 407−413.
7. Feany, M. B., and Dickson, D. W. (1995) Widespread cytoskeletal pathology characterizes corticobasal degeneration, *Am. J. Pathol. 146*, 1388−1396.
8. Murayama, S., Mori, H., Ihara, Y., and Tomonaga, M. (1990) Immunocytochemical and ultrastructural studies of Pick's disease, *Ann. Neurol. 27*, 394−405.
9. Wisniewski, K., Jervis, G. A., Moretz, R. C., and Wisniewski, H. M. (1979) Alzheimer neurofibrillary tangles in diseases other than senile and presenile dementia, *Ann. Neurol. 5*, 288−294.
10. Papasozomenos, S. C. (1989) Tau protein immunoreactivity in dementia of the Alzheimer type. I. Morphology, evolution, distribution, and pathogenetic implications, *Lab. Invest. 60*, 123−137.
11. Spillantini, M. G., Goedert, M., Crowther, R. A., Murrell, J. R., Farlow, M. R., and Ghetti, B. (1997) Familial multiple system tauopathy with presenile dementia: a disease with abundant neuronal and glial tau filaments, *Proc. Natl. Acad. Sci. U.S.A. 94*, 4113−4118.
12. Grundke-Iqbal, I., Iqbal, K., Tung, Y. C., Quinlan, M., Wisniewski, H. M., and Binder, L. I. (1986) Abnormal phosphorylation of the microtubule-associated protein tau (tau) in Alzheimer cytoskeletal pathology, *Proc. Natl. Acad. Sci. U.S.A. 83*, 4913−4917.
13. Wood, J. G., Mirra, S. S., Pollock, N. J., and Binder, L. I. (1986) Neurofibrillary tangles of Alzheimer disease share antigenic determinants with the axonal microtubule-associated protein tau (tau), *Proc. Natl. Acad. Sci. U.S.A. 83*, 4040−4043.
14. Alonso, A. C., Grundke-Iqbal, I., and Iqbal, K. (1996) Alzheimer's disease hyperphosphorylated tau sequesters normal tau into tangles of filaments and disassembles microtubules, *Nat. Med. 2*, 783−787.
15. Yan, S. D., Chen, X., Schmidt, A. M., Brett, J., Godman, G., Zou, Y. S., Scott, C. W., Caputo, C., Frappier, T., Smith, M. A., et al. (1994) Glycated tau protein in Alzheimer disease: a mechanism for induction of oxidant stress, *Proc. Natl. Acad. Sci. U.S.A. 91*, 7787−7791.
16. Gamblin, T. C., Chen, F., Zambrano, A., Abraha, A., Lagalwar, S., Guillozet, A. L., Lu, M., Fu, Y., Garcia-Sierra, F., LaPointe, N., Miller, R., Berry, R. W., Binder, L. I., and Cryns, V. L. (2003) Caspase cleavage of tau: linking amyloid and neurofibrillary tangles in Alzheimer's disease, *Proc. Natl. Acad. Sci. U.S.A. 100*, 10032−10037.
17. Ghoshal, N., Garcia-Sierra, F., Fu, Y., Beckett, L. A., Mufson, E. J., Kuret, J., Berry, R. W., and Binder, L. I. (2001) Tau-66: evidence for a novel tau conformation in Alzheimer's disease, *J. Neurochem. 77*, 1372−1385.
18. Ghoshal, N., Garcia-Sierra, F., Wuu, J., Leurgans, S., Bennett, D. A., Berry, R. W., and Binder, L. I. (2002) Tau conformational changes correspond to impairments of episodic memory in mild cognitive impairment and Alzheimer's disease, *Exp. Neurol. 177*, 475−493.
19. Garcia-Sierra, F., Ghoshal, N., Quinn, B., Berry, R. W., and Binder, L. I. (2003) Conformational changes and truncation of tau protein during tangle evolution in Alzheimer's disease, *J. Alzheimer's Dis. 5*, 65−77.
20. Beckman, J. S. (1996) Oxidative damage and tyrosine nitration from peroxynitrite, *Chem. Res. Toxicol. 9*, 836−844.
21. Reynolds, M. R., Berry, R. W., and Binder, L. I. (2005) Site-specific nitration and oxidative dityrosine bridging of the tau protein by peroxynitrite: Implications for Alzheimer's disease, *Biochemistry 44*, 1690−1700.
22. Souza, J. M., Giasson, B. I., Chen, Q., Lee, V. M., and Ischiropoulos, H. (2000) Dityrosine cross-linking promotes formation of stable alpha-synuclein polymers. Implication of nitrative and oxidative stress in the pathogenesis of neurodegenerative synucleinopathies, *J. Biol. Chem. 275*, 18344−18349.
23. Ischiropoulos, H. (2003) Biological selectivity and functional aspects of protein tyrosine nitration, *Biochem. Biophys. Res. Commun. 305*, 776−783.
24. Souza, J. M., Daikhin, E., Yudkoff, M., Raman, C. S., and Ischiropoulos, H. (1999) Factors determining the selectivity of protein tyrosine nitration, *Arch. Biochem. Biophys. 371*, 169−178.
25. Greenacre, S. A., and Ischiropoulos, H. (2001) Tyrosine nitration: localisation, quantification, consequences for protein function and signal transduction, *Free Radical Res. 34*, 541−581.
26. MacMillan-Crow, L. A., Crow, J. P., and Thompson, J. A. (1998) Peroxynitrite-mediated inactivation of manganese superoxide

dismutase involves nitration and oxidation of critical tyrosine residues, *Biochemistry 37*, 1613−1622.
27. Guittet, O., Decottignies, P., Serani, L., Henry, Y., Le Marechal, P., Laprevote, O., and Lepoivre, M. (2000) Peroxynitrite-mediated nitration of the stable free radical tyrosine residue of the ribonucleotide reductase small subunit, *Biochemistry 39*, 4640−4648.
28. Yamakura, F., Taka, H., Fujimura, T., and Murayama, K. (1998) Inactivation of human manganese-superoxide dismutase by peroxynitrite is caused by exclusive nitration of tyrosine 34 to 3-nitrotyrosine, *J. Biol. Chem. 273*, 14085−14089.
29. Ara, J., Przedborski, S., Naini, A. B., Jackson-Lewis, V., Trifiletti, R. R., Horwitz, J., and Ischiropoulos, H. (1998) Inactivation of tyrosine hydroxylase by nitration following exposure to peroxynitrite and 1-methyl-4-phenyl-1,2,3,6-tetrahydropyridine (MPTP), *Proc. Natl. Acad. Sci. U.S.A. 95*, 7659−7663.
30. Blanchard-Fillion, B., Souza, J. M., Friel, T., Jiang, G. C., Vrana, K., Sharov, V., Barron, L., Schoneich, C., Quijano, C., Alvarez, B., Radi, R., Przedborski, S., Fernando, G. S., Horwitz, J., and Ischiropoulos, H. (2001) Nitration and inactivation of tyrosine hydroxylase by peroxynitrite, *J. Biol. Chem. 276*, 46017−46023.
31. Uversky, V. N., Yamin, G., Munishkina, L. A., Karymov, M. A., Millett, I. S., Doniach, S., Lyubchenko, Y. L., and Fink, A. L. (2005) Effects of nitration on the structure and aggregation of alpha-synuclein, *Brain. Res. Mol. Brain Res. 134*, 84−102.
32. Yamin, G., Uversky, V. N., and Fink, A. L. (2003) Nitration inhibits fibrillation of human alpha-synuclein in vitro by formation of soluble oligomers, *FEBS Lett. 542*, 147−152.
33. Alim, M. A., Ma, Q. L., Takeda, K., Aizawa, T., Matsubara, M., Nakamura, M., Asada, A., Saito, T., Kaji, H., Yoshii, M., Hisanaga, S., and Ueda, K. (2004) Demonstration of a role for alpha-synuclein as a functional microtubule-associated protein, *J. Alzheimer's Dis. 6*, 435−442; discussion 443−449.
34. Giasson, B. I., Duda, J. E., Murray, I. V., Chen, Q., Souza, J. M., Hurtig, H. I., Ischiropoulos, H., Trojanowski, J. Q., and Lee, V. M. (2000) Oxidative damage linked to neurodegeneration by selective alpha-synuclein nitration in synucleinopathy lesions, *Science 290*, 985−989.
35. Horiguchi, T., Uryu, K., Giasson, B. I., Ischiropoulos, H., LightFoot, R., Bellmann, C., Richter-Landsberg, C., Lee, V. M., and Trojanowski, J. Q. (2003) Nitration of tau protein is linked to neurodegeneration in tauopathies, *Am. J. Pathol. 163*, 1021−1031.
36. Carmel, G., Mager, E. M., Binder, L. I., and Kuret, J. (1996) The structural basis of monoclonal antibody Alz50's selectivity for Alzheimer's disease pathology, *J. Biol. Chem. 271*, 32789−32795.
37. Lee, G., Cowan, N., and Kirschner, M. (1988) The primary structure and heterogeneity of tau protein from mouse brain, *Science 239*, 285−288.
38. Kosik, K. S., Orecchio, L. D., Binder, L., Trojanowski, J. Q., Lee, V. M., and Lee, G. (1988) Epitopes that span the tau molecule are shared with paired helical filaments, *Neuron 1*, 817−825.
39. Goedert, M., Spillantini, M. G., Jakes, R., Rutherford, D., and Crowther, R. A. (1989) Multiple isoforms of human microtubule-associated protein tau: sequences and localization in neurofibrillary tangles of Alzheimer's disease, *Neuron 3*, 519−526.
40. Studier, F. W., Rosenberg, A. H., Dunn, J. J., and Dubendorff, J. W. (1990) Use of T7 RNA polymerase to direct expression of cloned genes, *Methods Enzymol. 185*, 60−89.
41. Abraha, A., Ghoshal, N., Gamblin, T. C., Cryns, V., Berry, R. W., Kuret, J., and Binder, L. I. (2000) C-terminal inhibition of tau assembly in vitro and in Alzheimer's disease, *J. Cell Sci. 113* (Part 21), 3737−3745.
42. Beckman, J. S., Chen, J., Ischiropoulos, H., and Crow, J. P. (1994) Oxidative chemistry of peroxynitrite, *Methods Enzymol. 233*, 229−240.
43. Uppu, R. M., Squadrito, G. L., Cueto, R., and Pryor, W. A. (1996) Selecting the most appropriate synthesis of peroxynitrite, *Methods Enzymol. 269*, 285−296.
44. Lowry, O. H., Rosebrough, N. J., Farr, A. L., and Randall, R. J. (1951) Protein measurement with the Folin phenol reagent, *J. Biol. Chem. 193*, 265−275.
45. Ischiropoulos, H., and al-Mehdi, A. B. (1995) Peroxynitrite-mediated oxidative protein modifications, *FEBS Lett. 364*, 279−282.
46. Gamblin, T. C., King, M. E., Dawson, H., Vitek, M. P., Kuret, J., Berry, R. W., and Binder, L. I. (2000) In vitro polymerization of tau protein monitored by laser light scattering: method and application to the study of FTDP-17 mutants, *Biochemistry 39*, 6136−6144.
47. King, M. E., Gamblin, T. C., Kuret, J., and Binder, L. I. (2000) Differential assembly of human tau isoforms in the presence of arachidonic acid, *J. Neurochem. 74*, 1749−1757.
48. Gamblin, T. C., King, M. E., Kuret, J., Berry, R. W., and Binder, L. I. (2000) Oxidative regulation of fatty acid-induced tau polymerization, *Biochemistry 39*, 14203−14210.
49. Gamblin, T. C., Berry, R. W., and Binder, L. I. (2003) Tau polymerization: role of the amino terminus, *Biochemistry 42*, 2252−2257.
50. Berry, R. W., Abraha, A., Lagalwar, S., LaPointe, N., Gamblin, T. C., Cryns, V. L., and Binder, L. I. (2003) Inhibition of tau polymerization by its carboxy-terminal caspase cleavage fragment, *Biochemistry 42*, 8325−8331.
51. Friguet, B., Chaffotte, A. F., Djavadi-Ohaniance, L., and Goldberg, M. E. (1985) Measurements of the true affinity constant in solution of antigen−antibody complexes by enzyme-linked immunosorbent assay, *J. Immunol. Methods 77*, 305−319.
52. Dahlquist, F. W. (1978) The meaning of Scatchard and Hill plots, *Methods Enzymol. 48*, 270−299.
53. Wilson, D. M., and Binder, L. I. (1997) Free fatty acids stimulate the polymerization of tau and amyloid beta peptides. In vitro evidence for a common effector of pathogenesis in Alzheimer's disease, *Am. J. Pathol. 150*, 2181−2195.
54. King, M. E., Ahuja, V., Binder, L. I., and Kuret, J. (1999) Ligand-dependent tau filament formation: implications for Alzheimer's disease progression, *Biochemistry 38*, 14851−14859.
55. von Bergen, M., Friedhoff, P., Biernat, J., Heberle, J., Mandelkow, E. M., and Mandelkow, E. (2000) Assembly of tau protein into Alzheimer paired helical filaments depends on a local sequence motif ((306)VQIVYK(311)) forming beta structure, *Proc. Natl. Acad. Sci. U.S.A. 97*, 5129−5134.
56. Evans, K. C., Berger, E. P., Cho, C. G., Weisgraber, K. H., and Lansbury, P. T., Jr. (1995) Apolipoprotein E is a kinetic but not a thermodynamic inhibitor of amyloid formation: implications for the pathogenesis and treatment of Alzheimer disease, *Proc. Natl. Acad. Sci. U.S.A. 92*, 763−767.
57. Harper, J. D., and Lansbury, P. T., Jr. (1997) Models of amyloid seeding in Alzheimer's disease and scrapie: mechanistic truths and physiological consequences of the time-dependent solubility of amyloid proteins, *Annu. Rev. Biochem. 66*, 385−407.
58. Hyman, B. T., Van Hoesen, G. W., Wolozin, B. L., Davies, P., Kromer, L. J., and Damasio, A. R. (1988) Alz-50 antibody recognizes Alzheimer-related neuronal changes, *Ann. Neurol. 23*, 371−379.
59. Wolozin, B. L., Pruchnicki, A., Dickson, D. W., and Davies, P. (1986) A neuronal antigen in the brains of Alzheimer patients, *Science 232*, 648−650.
60. LoPresti, P., Szuchet, S., Papasozomenos, S. C., Zinkowski, R. P., and Binder, L. I. (1995) Functional implications for the microtubule-associated protein tau: localization in oligodendrocytes, *Proc. Natl. Acad. Sci. U.S.A. 92*, 10369−10373.
61. Chirita, C. N., Necula, M., and Kuret, J. (2003) Anionic micelles and vesicles induce tau fibrillization in vitro, *J. Biol. Chem. 278*, 25644−25650.
62. Chirita, C. N., and Kuret, J. (2004) Evidence for an intermediate in tau filament formation, *Biochemistry 43*, 1704−1714.
63. Kuret, J., Chirita, C. N., Congdon, E. E., Kannanayakal, T., Li, G., Necula, M., Yin, H., and Zhong, Q. (2005) Pathways of tau fibrillization, *Biochim. Biophys. Acta 1739*, 167−178.
64. Trinczek, B., Ebneth, A., Mandelkow, E. M., and Mandelkow, E. (1999) Tau regulates the attachment/detachment but not the speed of motors in microtubule-dependent transport of single vesicles and organelles, *J. Cell Sci. 112* (Part 14), 2355−2367.
65. Seitz, A., Kojima, H., Oiwa, K., Mandelkow, E. M., Song, Y. H., and Mandelkow, E. (2002) Single-molecule investigation of the interference between kinesin, tau and MAP2c, *EMBO J. 21*, 4896−4905.
66. Brandt, R., Leger, J., and Lee, G. (1995) Interaction of tau with the neural plasma membrane mediated by tau's amino-terminal projection domain, *J. Cell Biol. 131*, 1327−1340.
67. Gray, E. G., Paula-Barbosa, M., and Roher, A. (1987) Alzheimer's disease: paired helical filaments and cytomembranes, *Neuropathol. Appl. Neurobiol. 13*, 91−110.
68. Oosawa, F., and Kasai, M. (1962) A theory of linear and helical aggregations of macromolecules, *J. Mol. Biol. 4*, 10−21.

69. Otvos, L., Jr., Feiner, L., Lang, E., Szendrei, G. I., Goedert, M., and Lee, V. M. (1994) Monoclonal antibody PHF-1 recognizes tau protein phosphorylated at serine residues 396 and 404, *J. Neurosci. Res. 39*, 669−673.
70. Derkinderen, P., Scales, T. M., Hanger, D. P., Leung, K. Y., Byers, H. L., Ward, M. A., Lenz, C., Price, C., Bird, I. N., Perera, T., Kellie, S., Williamson, R., Noble, W., Van Etten, R. A., Leroy, K., Brion, J. P., Reynolds, C. H., and Anderton, B. H. (2005) Tyrosine 394 is phosphorylated in Alzheimer's paired helical filament tau and in fetal tau with c-Abl as the candidate tyrosine kinase, *J. Neurosci. 25*, 6584−6593.
71. Mandelkow, E. M., Schweers, O., Drewes, G., Biernat, J., Gustke, N., Trinczek, B., and Mandelkow, E. (1996) Structure, microtubule interactions, and phosphorylation of tau protein, *Ann. N.Y. Acad. Sci. 777*, 96−106.
72. Gamblin, T. C., Berry, R. W., and Binder, L. I. (2003) Modeling tau polymerization in vitro: a review and synthesis, *Biochemistry 42*, 15009−15017.
73. Akiyama, H., Barger, S., Barnum, S., Bradt, B., Bauer, J., Cole, G. M., Cooper, N. R., Eikelenboom, P., Emmerling, M., Fiebich, B. L., Finch, C. E., Frautschy, S., Griffin, W. S., Hampel, H., Hull, M., Landreth, G., Lue, L., Mrak, R., Mackenzie, I. R., McGeer, P. L., O'Banion, M. K., Pachter, J., Pasinetti, G., Plata-Salaman, C., Rogers, J., Rydel, R., Shen, Y., Streit, W., Strohmeyer, R., Tooyoma, I., Van Muiswinkel, F. L., Veerhuis, R., Walker, D., Webster, S., Wegrzyniak, B., Wenk, G., and Wyss-Coray, T. (2000) Inflammation and Alzheimer's disease, *Neurobiol. Aging 21*, 383−421.
74. Goodwin, J. L., Uemura, E., and Cunnick, J. E. (1995) Microglial release of nitric oxide by the synergistic action of beta-amyloid and IFN-gamma, *Brain Res. 692*, 207−214.
75. Ii, M., Sunamoto, M., Ohnishi, K., and Ichimori, Y. (1996) beta-Amyloid protein-dependent nitric oxide production from microglial cells and neurotoxicity, *Brain Res. 720*, 93−100.
76. Luth, H. J., Munch, G., and Arendt, T. (2002) Aberrant expression of NOS isoforms in Alzheimer's disease is structurally related to nitrotyrosine formation, *Brain Res. 953*, 135−143.
77. Good, P. F., Werner, P., Hsu, A., Olanow, C. W., and Perl, D. P. (1996) Evidence of neuronal oxidative damage in Alzheimer's disease, *Am. J. Pathol. 149*, 21−28.
78. Smith, M. A., Richey Harris, P. L., Sayre, L. M., Beckman, J. S., and Perry, G. (1997) Widespread peroxynitrite-mediated damage in Alzheimer's disease, *J. Neurosci. 17*, 2653−2657.
79. Markesbery, W. R., and Carney, J. M. (1999) Oxidative alterations in Alzheimer's disease, *Brain Pathol. 9*, 133−146.
80. Drechsel, D. N., Hyman, A. A., Cobb, M. H., and Kirschner, M. W. (1992) Modulation of the dynamic instability of tubulin assembly by the microtubule-associated protein tau, *Mol. Biol. Cell 3*, 1141−1154.
81. Bramblett, G. T., Goedert, M., Jakes, R., Merrick, S. E., Trojanowski, J. Q., and Lee, V. M. (1993) Abnormal tau phosphorylation at Ser396 in Alzheimer's disease recapitulates development and contributes to reduced microtubule binding, *Neuron 10*, 1089−1099.
82. Zhang, Y. J., Xu, Y. F., Chen, X. Q., Wang, X. C., and Wang, J. Z. (2005) Nitration and oligomerization of tau induced by peroxynitrite inhibit its microtubule-binding activity, *FEBS Lett. 579*, 2421−2427.

BI051028W